atmosphere

MDPI

Article

Impact of Stratospheric Aerosol Geoengineering on Meteorological Droughts in West Africa

Adéchina Eric Alamou [1,2,*], Ezéchiel Obada [1,2], Eliézer Iboukoun Biao [1,2], Esdras Babadjidé Josué Zandagba [1,2], Casimir Y. Da-Allada [1,3], Frederic K. Bonou [3], Ezinvi Baloïtcha [3], Simone Tilmes [4] and Peter J. Irvine [5]

1 Laboratory of Geosciences, Environment and Applications, National University of Sciences Technology, Engineering and Mathematics, Abomey-Calavi BP 2282, Benin; obada.ezechiel@unstim.bj (E.O.); biaoeliezer@unstim.bj (E.I.B.); zandagbajosue@unstim.bj (E.B.J.Z.); da.casimir@unstim.bj (C.Y.D.-A.)
2 Laboratory of Applied Hydrology, National Water Institute, University of Abomey-Calavi, Abomey-Calavi BP 2549, Benin
3 International Chair in Mathematical Physics and Applications (ICMPA—UNESCO CHAIR), University of Abomey-Calavi, Abomey-Calavi BP 2549, Benin; fredericbonou@unstim.bj (F.K.B.); ezinvi_boaloitcha@cipma.net (E.B.)
4 National Center for Atmospheric Research, Boulder, CO 80305, USA; tilmes@ucar.edu
5 Earth Sciences, University College London, London WC1E 6BT, UK; p.irvine@ucl.ac.uk
* Correspondence: ericalamou@unstim.bj

Abstract: This study assesses changes in meteorological droughts in West Africa under a high greenhouse gas scenario, i.e., a representative concentration pathway 8.5 (RCP8.5), and under a scenario of stratospheric aerosol geoengineering (SAG) deployment. Using simulations from the Geoengineering Large Ensemble (GLENS) project that employed stratospheric sulfate aerosols injection to keep global mean surface temperature, as well as the interhemispheric and equator-to-pole temperature gradients at the 2020 level (present-day climate), we investigated the impact of SAG on meteorological droughts in West Africa. Analysis of the meteorological drought characteristics (number of drought events, drought duration, maximum length of drought events, severity of the greatest drought events and intensity of the greatest drought event) revealed that over the period from 2030–2049 and under GLENS simulations, these drought characteristics decrease in most regions in comparison to the RCP8.5 scenarios. On the contrary, over the period from 2070–2089 and under GLENS simulations, these drought characteristics increase in most regions compared to the results from the RCP8.5 scenarios. Under GLENS, the increase in drought characteristics is due to a decrease in precipitation. The decrease in precipitation is largely driven by weakened monsoon circulation due to the reduce of land–sea thermal contrast in the lower troposphere.

Keywords: stratospheric aerosol geoengineering; climate change; GLENS simulations; meteorological droughts; West Africa

Citation: Alamou, A.E.; Obada, E.; Biao, E.I.; Zandagba, E.B.J.; Da-Allada, C.Y.; Bonou, F.K.; Baloïtcha, E.; Tilmes, S.; Irvine, P.J. Impact of Stratospheric Aerosol Geoengineering on Meteorological Droughts in West Africa. *Atmosphere* **2022**, *13*, 234. https://doi.org/10.3390/atmos13020234

Academic Editors: Baojie He, Ayyoob Sharifi, Chi Feng and Jun Yang

Received: 16 December 2021
Accepted: 25 January 2022
Published: 29 January 2022

1. Introduction

Climate change and accelerated population growth have become the key limiting factors for sustainable human resources development and natural systems conservation [1]. As global warming increases, the magnitude of climate change impacts on the environment and society increases [1,2], while the rapidly increasing population is challenging the food security of the world's current population of 7.6 billion, which is projected to be 9.8 and 11.2 billion in 2050 and 2100, respectively [1,3]. Increasing temperature leads to an increase in specific humidity, wind speed and precipitation [4–6]. However, [5] shows that global-scale relative humidity is decreasing in the last decades with increasing temperature. Under the high anthropogenic greenhouse gas emission scenario (RCP8.5), increasing temperature can increase the rates of hydrologic system losses to evaporation and transpiration and, in turn, produce more rainfall [7]. Therefore, the Intergovernmental Panel on Climate

Change (IPCC) have noted a widespread point of view of climate scientists that events (e.g., droughts and floods) now regarded as extremes are projected to become more frequent and widespread in the future [8].

Based on volcanic eruptions, it was shown that stratospheric aerosols have the potential to cool the planet [9,10]. Solar radiation management (SRM), a set of proposals to artificially reduce the amount of solar radiation reaching the surface of the Earth, has been suggested as complementary approach to reducing the risks of global warming alongside more conventional approaches [11–14]. Stratospheric aerosol geoengineering (SAG), one of the SRM methods, offers a unique potential to rapidly lower global temperatures ([10,13,15,16]). At regional scale, ref. [17] indicated that under SAG, future extreme temperature indices are closer to present day indices over Africa. However, if SAG is projected to offset all warming with regard to the present day or to the near past period, it could weaken the hydrological cycle, potentially more than off-setting the increase expected under global warming, which might increase climate risks for some regions [11,18–20]. Many studies, in fact, indicate a decrease in the pole-to-equator temperature gradient relative to a case without elevated CO_2, and there would be a slowdown of the hydrologic cycle, including a decrease in global mean and annual mean precipitation [18,20–22].

West Africa is particularly vulnerable to climate change due to its high climate variability, its high reliance on rain-fed agriculture, and its limited economic and institutional capacity to respond to climate variability and change [23]. As most people in West Africa are involved in climate-sensitive sectors of the economy, any change in the climate that enhances drier conditions may increase the vulnerability to climate risks over the region. Any substantial rainfall deficit usually devastates socio-economic activities for a long period because agriculture, hydro-electric power, and river basin management depend on rainfall [24]. Recurrent drought is a complex phenomenon that may adversely affect water supplies and crop and livestock production, causing food insecurity and the disruption of the livelihood activities of a region [25–27].

Some studies assessed the impact of climate change on drought in West Africa and others regions of Africa. To better understand climate change and drought perceptions in the rural Savannah in West Africa, ref. [28] noticed that the timing and spatial distribution of precipitation have continued to vary significantly, and the high rainfall variability is coupled with intra-seasonal dry spells (agricultural and meteorological drought), which have become frequent, prolonged and severe. Drought areas in East Africa are likely to increase at the end of the 21st century by 16%, 36%, and 54% under Representative Concentration Pathways (RCPs) 2.6, 4.5, and 8.5, respectively, with the areas affected by extreme drought increasing more rapidly than severe and moderate droughts [1]. Indeed, an increase in drought intensity and spatial extent are projected related to the present-day over the Volta River Basin using standardized precipitation index (SPI) and the standardized precipitation and evapotranspiration index (SPEI) using an ensemble of climate models under climate change scenarios [27]. Drought frequency (events per decade) may be magnified by a factor of 1.2 (2046–2065) to 1.6 (2081–2100) compared to the present-day episodes in the basin [24,27]. They also projected an increase in the magnitude and frequency of severe droughts over both the Niger River and Volta River basins at all global warming levels. More than 75% of the simulations agree on the projected increase at the 1.5 global warming level, and all simulations agree on the increase at higher global warming levels. The projected intensification of drought characteristics under climate change scenarios and the weakness of hydrological cycle under SAG call on us to adopt adequate mitigation and resilience measures to face the severe consequences of drought in the West Africa. As a reminder, the Sahelian drought of the 1970s–1990s was one of the largest humanitarian disasters of the past 50 years, causing up to 250,000 deaths and creating 10 million refugees [29]. The origin of this drought is not yet unanimous among researchers, but recently, ref. [29] showed that sporadic volcanic eruptions in the Northern Hemisphere also strongly influence the Atlantic Sea surface temperature gradient and cause Sahelian droughts. They conclude that further studies of the detailed regional impacts on the Sahel

and other vulnerable areas are required to inform policymakers in developing careful consensual global governance before any practical SRM geoengineering scheme is implemented. In this context, it is important to investigate how climate change and SAG would impact projected droughts in West Africa. No study has been conducted yet on the impact of SAG on drought in West Africa.

The objective of this paper is to use Geoengineering Large Ensembles (GLENS) simulations [18] to improve our understanding on the potential impact of SAG on meteorological drought in West Africa.

2. Data and Methods

2.1. Study Area

West Africa extends from 4° to 28° North latitude and from 17° West longitude to 16° East longitude (Figure 1). It covers an area of 6 million Km^2 with the Gulf of Guinea as its southern boundary [30]. Annual precipitation varies from about 250 mm at the desert area to over 2000 mm near the coastal zone [23]. The annual average minimum daily temperature is between 16 and 20 °C, while the annual average of maximum daily temperature varies from 27 °C to 35 °C [31].

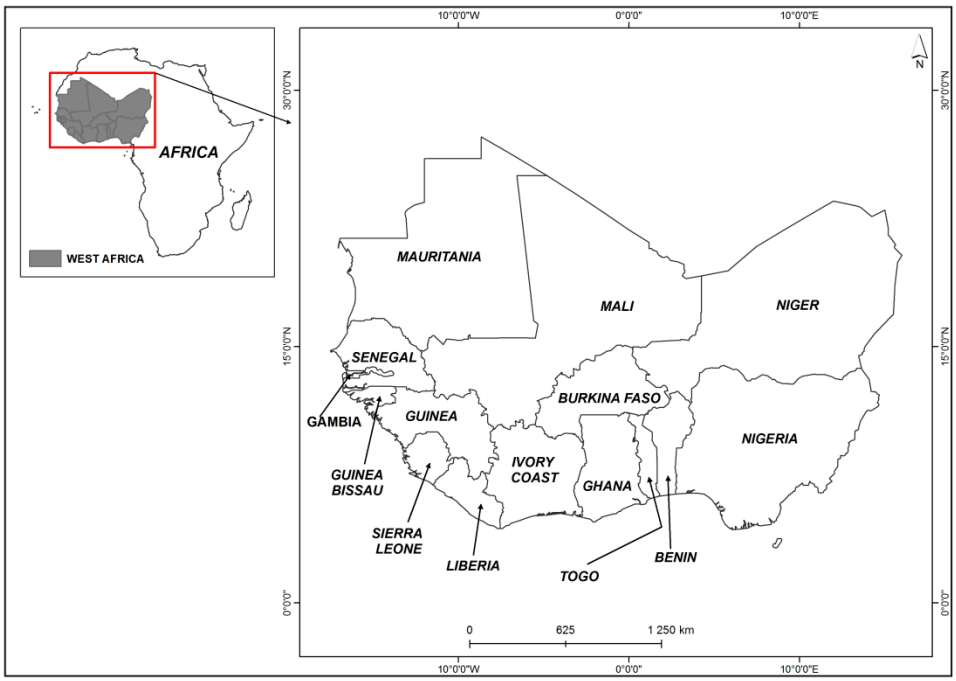

Figure 1. West Africa region.

2.2. Data

We used observed and satellite datasets of CPC Global PRCP V1.0; (https://www.esrl.noaa.gov/psd/data/gridded/data.cpc.globalprecip.html, access on 20 January 2020) and model data from the Geoengineering Large Ensemble (GLENS) project [16]. CPC Global PRCP are daily data with 0.5° longitude × 0.5° latitude spatial resolution. GLENS simulations are grid monthly data with 0.95° longitude × 1.25° latitude resolution. It uses prescribed greenhouse gas forcing concentrations following the representative concentration pathway 8.5 (RCP8.5, i.e., a high anthropogenic emission scenario) [24]. These simulations were conducted using the NCAR Community Earth System Model with the Whole Atmosphere Community Climate Model as its atmospheric component (CESM1 WACCM) [32] (Table 1).

Table 1. Summary of available model simulations used in this study.

Simulations	Year	Ensemble Members
Historical	1981–2010	1 (001)
RCP8.5	2010–2097	4 (001–003; 021)
GLENS	2031–2097	4 (001–003; 021)

2.3. Methods

To define drought events and assess their durations, severities, intensities and ex-tents, standardized precipitation indices were used. SPI is classically derived by fitting a gamma probability distribution function to precipitation. It has been shown that precipitation is highly heavy tailed [33], and [34,35] stated that the values of SPI are quite sensitive to the choice of parametric distribution function, particularly in the tail of the distribution. For long-term data sets, necessary for drought assessment, typically different empirical methods lead to similar results [36]. There are also alternative methods for deriving empirical probabilities such that they can be used for deriving nonparametric SPI. To avoid the sensitivity of parameter choice on SPI, we computed the marginal probability of precipitation [37] using the empirical Gringorten plotting position [38], Equation (1), and fitting it with Gaussian distribution Equation (2):

$$p(x_i) = \frac{i - 0.44}{n + 0.12} \tag{1}$$

where n is the sample size, i denotes the rank of non-zero precipitation data from the smallest sample, and $p(x_i)$ is the corresponding empirical probability.

The outputs of Equation (1) are then transformed into a Standardized Precipitation Index (SPI) as:

$$\text{SPI} = \phi^{-1}(p) \tag{2}$$

where ϕ is the standard normal distribution function, and p is the probability derived from Equation (1).

A drought event is defined as a period over which SPI is continuously less than -0.5. Twelve months of SPI were investigated.

The drought classification scheme used in this study is detailed in Table 2.

Table 2. Drought severity information in both the original standardized scale and their corresponding drought scale [39].

SPI	Drought Scale	Description
−0.50 to −0.79	D_0	Abnormally dry
−0.80 to −1.29	D_1	Moderate drought
−1.30 to −1.59	D_2	Severe drought
−1.60 to –1.99	D_3	Extreme drought
−2.00 or less	D_4	Exceptional drought

We used 6 drought characteristics to analyze the drought pattern in West Africa. These drought characteristics are: the average number of drought events (N), the average length of drought events (DL), the drought extend area (DA), the length of the greatest drought event (MLD), its severity (DS) and its intensity (DI). The greatest drought is the drought event with the maximum length.

DA (%) is computed as the percent of West Africa area under drought condition for each month:

$$\text{DA} = \frac{n_D}{n_T} \times 100 \tag{3}$$

where n_D is the number of grids with SPI less than -0.5 and n_T is the total grids over the study area. DS was calculated as:

$$\mathrm{DS} = \left| \sum_i^n (\mathrm{SPI} < -0.50) \right| \quad (4)$$

n is the length (in months) of greatest drought event.

DI was calculated as the mean drought severity over the greatest drought event:

$$\mathrm{DI} = \frac{|\sum_i^n (\mathrm{SPI} < -0.50)|}{n} \quad (5)$$

3. Results

3.1. Evaluation of Model Performance in Simulating Precipitation

In this section, we assess the performance of the CESM1 (WACCM) simulations to reproduce the observed precipitation in West Africa. The assessment of precipitation is very important because the accuracy and reliability of the future simulations of the meteorological drought index depend on how well the models capture the historical precipitation [24]. Figure 2 presents the spatial distribution of observed, simulated and observed-simulated seasonal and annual mean rainfall in West Africa. The model and the observation products show similar spatial precipitation patterns for each season. The rainfall distribution decreases northwards from the Guinea coast to the Sahel–Sahara region, However, During MAM (March-April-May), the model underestimates rainfall over West Africa by around 1 mm/day between 4 and 15° North latitude and around 0.25 mm/day after 15° North latitude. In the Sierra Leone and Liberia regions, the model overestimates rainfall by around 1 mm/day. During JJA (June-July-August), SON (September-October-November) and at an annual scale, the model overestimates rainfall in southern West Africa, while it underestimates rainfall in northern West Africa. The model overestimates rainfall by around 1 mm/day between 4° and 9° North latitude during JJA and between 4° and 15° North latitude during SON. At the annual scale, the model overestimates rainfall by around 0.5 to 1 mm/day in the coastal region of West Africa. These model biases over Sierra Leone and Liberia, located in mountainous areas, may be associated with the poor simulation of orographic forced ascent (e.g., [40,41]) or the large uncertainty in the model precipitation estimates over this region [41,42]. In general, the seasonality is well reproduced in most of the countries, except in Sierra Leone and Liberia, where high intensity was found in the GLENS simulations in most of the seasons.

3.2. Long Term Projected Drought

Figure 3 shows the comparison between the projected time series of SPI under RCP8.5 and the GLENS simulations. The projected SPI from the RCP8.5 scenario indicates an increasing trend of SPI from 2010 to 2097 due to the increasing trend of precipitation, while a decreasing trend is expected from GLENS simulations. It can also be seen that over the period 2030–2059, the SPI from RCP8.5 and GLENS are similar and are constituted by a frequent alternation between short periods of positive SPI and negative SPI. The negative SPI are usually greater than -0.5. It means that under both GLENS and RCP8.5 simulations, West Africa would not experience significant drought events in the period of 2030 to 2059. Over the period 2060–2097, SPI values are mostly negative under the GLENS simulation and mostly positive under the RCP8.5 scenario. This means that under the GLENS simulations, West Africa would be a wet region, while under RCP8.5 simulations, dry conditions would dominate in the region. Severe and extreme drought events would occur with the GLENS simulation over this period.

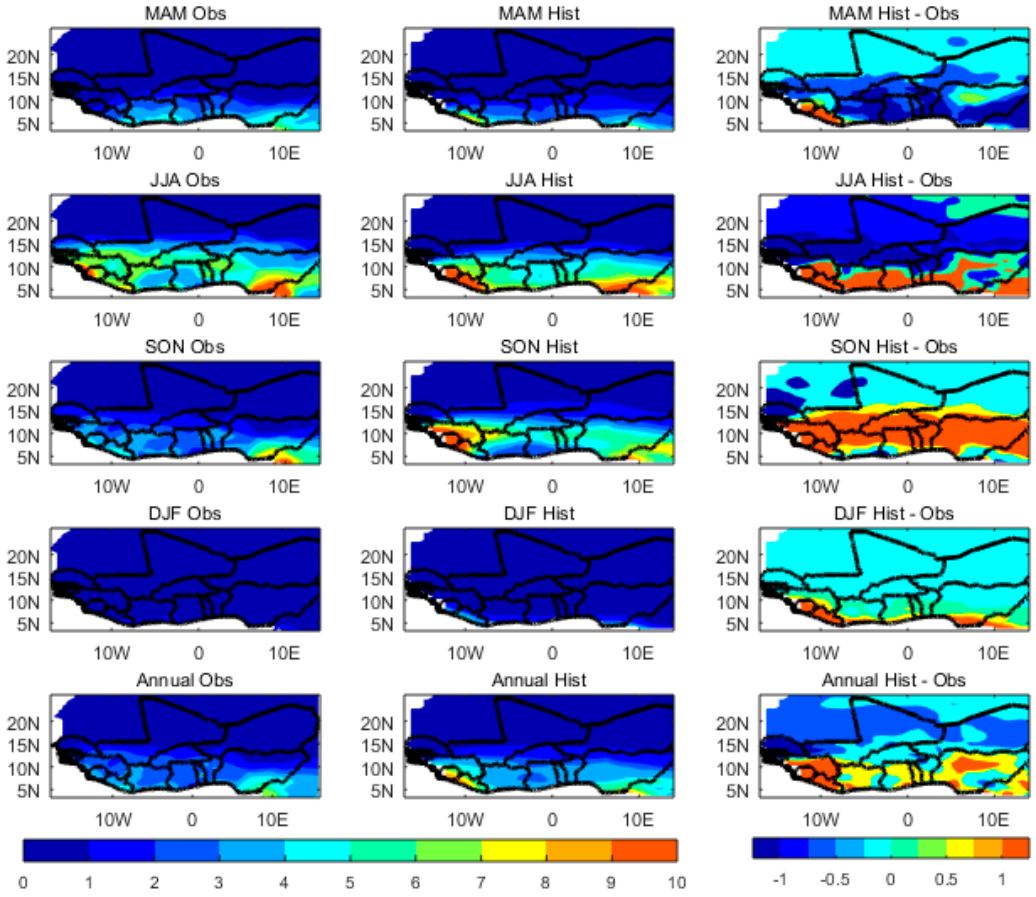

Figure 2. Seasonal and annual comparison of mean climatology of observed and simulated rainfall in West Africa (observed rainfall in first column, GLENS historic simulation in second column, and GLENS historic simulation minus observed rainfall in third column.

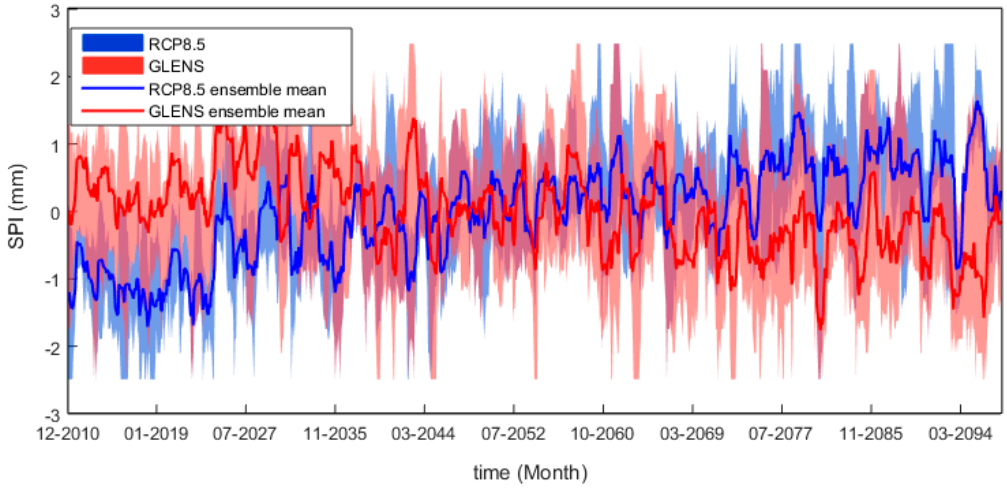

Figure 3. Comparison of projected time series of SPI under RCP8.5 and GLENS scenarios over West Africa.

In general, long-term projected drought indicates that the long-term injection of SO_2 in the stratosphere could induce in the second half of the century severe to extreme meteorological droughts in West Africa due to the decrease in precipitation.

3.3. Drought Characteristics

3.3.1. Mean Values of Drought Characteristics in West Africa over Different Periods

Table 3 shows the Mean values of drought characteristics in West Africa over different periods. Over the control period (CTRL) the values of the number of drought events, drought duration, the length of greatest drought, the severity of greatest drought and the intensity of the greatest drought are 4.60, 18.40, 34, 40.70 and 1.16, respectively. Over the projected 2030–2049 period, drought characteristics for the RCP8.5 and GLENS simulations are 6.59 and 4.68, respectively, for the number of drought events, 12.43 and 11.10 for the drought duration, 22.96 and 18.63 for the length of the greatest drought, 28.01 and 22.01 for the severity of greatest drought and 1.21 and 1.15 for the intensity of the greatest drought. The investigated drought characteristics of this period are similar for both the RCP8.5 and GLENS simulations, but these characteristics are slightly less than those of the CTRL period. Over the 2070–2089 period, scenario RCP8.5 indicates 2.15, 6.46, 9.15, 10.87 and 0.94 for the number of drought events, the drought duration, the length of the greatest drought, the severity of the greatest drought and the intensity of the greatest drought, respectively. These values are largely inferior to those of the CTRL period, indicating an attenuation of drought under RCP8.5 during 2070–2089 compared to the CTRL period. Drought characteristics during the period 2027–2089 and under GLENS are 6.11, 14.23, 28.72, 36.77 and 1.29 for the number of drought events, drought duration, the length of the greatest drought, the severity of the greatest drought and the intensity of the greatest drought, respectively. The number of drought events under GLENS (2070–2089) is greater than the number of events under the control period. However, the duration of these events under GLENS is less than their duration under the control period. The observation is made for the greatest drought characteristics, where the intensity of the greater drought event of GLENS is superior to those of the CTRL, but the length and the severity of this drought are less than those of CRTL.

Table 3. Mean values of drought characteristics in West Africa over different periods.

Period	Number of Drought Events	Drought Duration (Months)	Length of Greatest Drought (Months)	Severity of Greatest Drought	Intensity of Greatest Drought
CTRL (2010–2029)	4.60	18.40	34	40.70	1.16
RCP8.5_2030–2049	6.59	12.43	22.96	28.01	1.21
GLENS_2030–2049	4.68	11.10	18.63	22.19	1.15
RCP8.5_2070–2089	2.15	6.46	9.15	10.87	0.94
GLENS_2070–2089	7.11	14.23	28.72	36.77	1.29

3.3.2. Drought Area

The drought area (DA: percentage of area with SPI less to −0.5) and areas of different drought severity scale (D_0: abnormally dry; D_1: moderate drought; D_2: severe drought; D_3: extreme drought; D_4: exceptional drought) under RCP8.5 (blue line) and GLENS scenarios (red line) are shown in Figure 4. For DA, D_0, D_1, D_2, D_3 and D_4, the drought areas have a decreasing trend under RCP8.5 simulation and increasing trend under GLENS simulation. These trends are in line with the increasing trend under the RCP8.5 scenario and the decreasing trend under the GLENS simulation that were found for SPI in Figure 3. Drought areas are always higher over the first decades of a projected period than over the last decades under the RCP8.5 simulation. The inverse situation occurred with GLENS simulation. Over the 2030–2059 period, the percentage of drought area under D_0 would vary from 2.3% to 32%, with an average of 13.1% under the RCP8.5 scenario, while it would vary from 0.2% to 22% with an average of 7.1% under the GLENS simulation. Over the 2068–2097 period, the extended area of D_0 is expected to decrease under RCP8.5 and could vary from 0 to 21% with an average of 6.1%. Meanwhile, it is expected to increase under the

GLENS simulation. Under the GLENS simulation, D_0 is expected to vary from 2% to 26.4%, with an average of 13.8%. The same situation was found for other drought area scales.

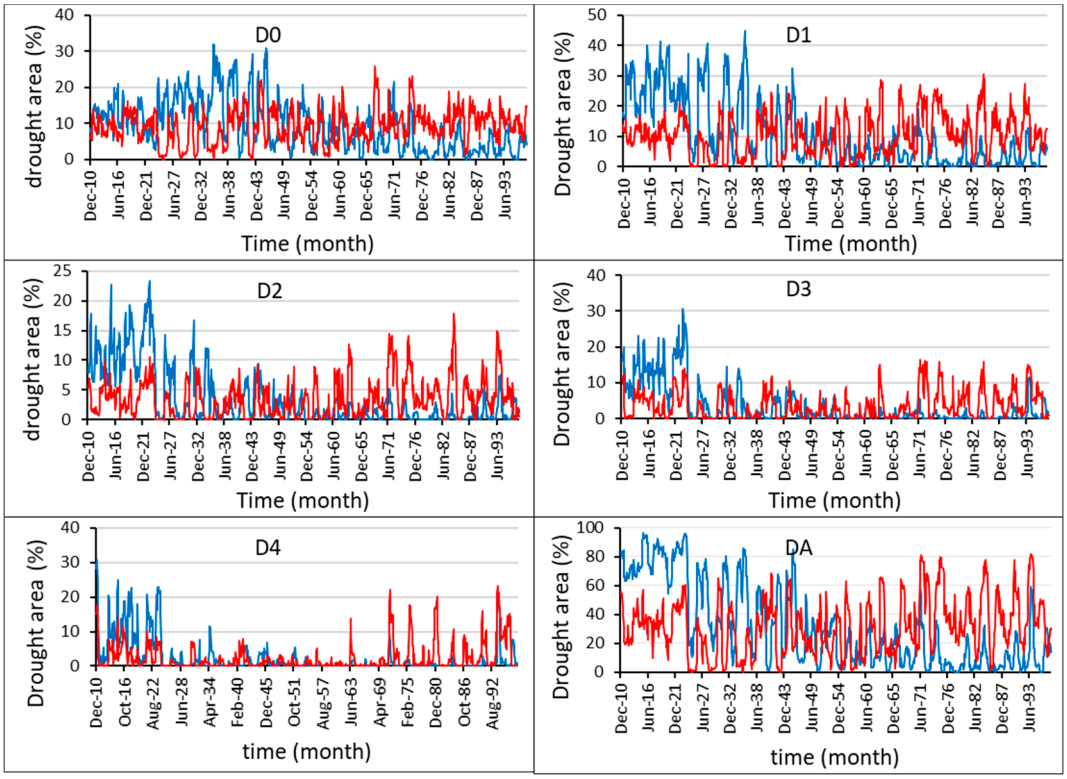

Figure 4. Evolution of Drought area in percentage (%) under RCP8.5 (blue line) and GLENS scenarios (red line) over West Africa.

3.3.3. Number of Drought Events

Over 2030–2049, the number of drought events under the GLENS scenarios is less than the number of drought events under RCP8.5 scenario. Indeed, under GLENS simulations, this number varies between 0 and 8 in most regions, except in northern Mauritania, northern Mali and northern Niger where this number can reach 12, while under the RCP8.5 simulations, the number of drought events varies from 5 to 20. The Guinea coast is the region has the maximum number of drought events under the RCP8.5 scenario.

On the contrary, over the period 2070–2089 and under the GLENS simulations, the number of drought events is higher than the number of drought events under the RCP8.5 scenario in most regions. The number of drought events under the GLENS simulations vary from 5 to 16. A high number of drought events were found in Mauritania, Burkina Faso, Ghana, the Ivory Coast, Liberia, South of Malia and Niger and in North of Nigeria, Benin. Under RCP8.5 simulations, the number of drought events varies from 0 to 15. A high number of drought events were found in Guinea, Sierra Leone and Liberia. This high number of drought events are around of 12 to 15. The remaining part of West Africa experiences low drought events which vary from 0 to 5.

Figure 5 depicted the change in the number of drought events under RCP8.5 and GLENS scenarios related to the Control period. Over the period 2030–2049 and under RCP8.5 simulations, the number of drought events could increase by two to eight related to the Control period (2010–2029) over Niger, Burkina Faso, Malia, Northern Nigeria and Benin, South of the Ivory Coast and Ghana, Liberia, South of Guinea and over Mauritania, while the remain part of West Africa could experience a slight decrease in the number of drought events (one to two events). Under the GLENS scenario, only the coastal region

of West Africa (up to 10° North latitude) could experience an increase of about six to eight events over 2030–2049 related to the Control period.

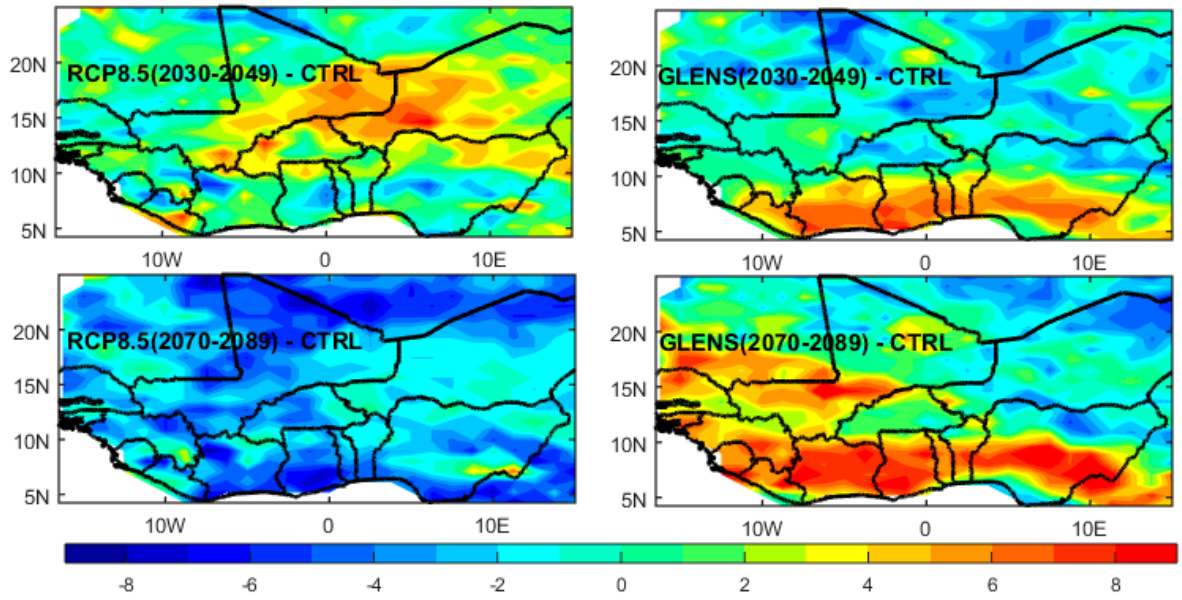

Figure 5. Change in the number of drought events under RCP8.5 and GLENS scenario related to Control period.

Over 2070–2089, a decrease in drought events could be expected in all West Africa under RCP8.5 related to the Control period, while under the GLENS scenario, an increase in the number of drought events could be expected over the coastal region between 4 to 10° North Latitude and over the Western part of the Sahelian region.

3.3.4. Drought Duration

Over the period 2030–2049 and under the GLENS simulations, the drought duration is smaller than the duration under the RCP8.5 scenarios. Indeed, under the GLENS simulations, this duration ranges between 0 and 15 months in most regions, whereas this duration can reach 25 months is some Sahelian regions under RCP8.5 scenarios. On the contrary, over the period 2070–2089 and under the GLENS simulations, the drought duration increases in most regions compared to the results from RCP8.5 scenarios. This duration can reach 25 months in some countries such as the Ivory Coast, Sierra Leone, Guinea, Senegal and Mali.

The change in the average drought duration under the RCP8.5 and GLENS scenarios related to the Control period is shown in Figure 6. The drought duration is expected to decrease under the RCP8.5 simulations over both the 2030–2049 and 2070–2089 projected periods related to the Control period in West Africa. This decrease could vary mostly from 5 to 12 months. Under GLENS, a decrease in drought duration is expected in Northern West Africa for both the 2030–2049 and 2070–2089 projected periods related to the Control period. For the Southern part of West Africa, an increase in drought duration is expected. This increase could be important over 2070–2089 compared to the 2030–2049 period.

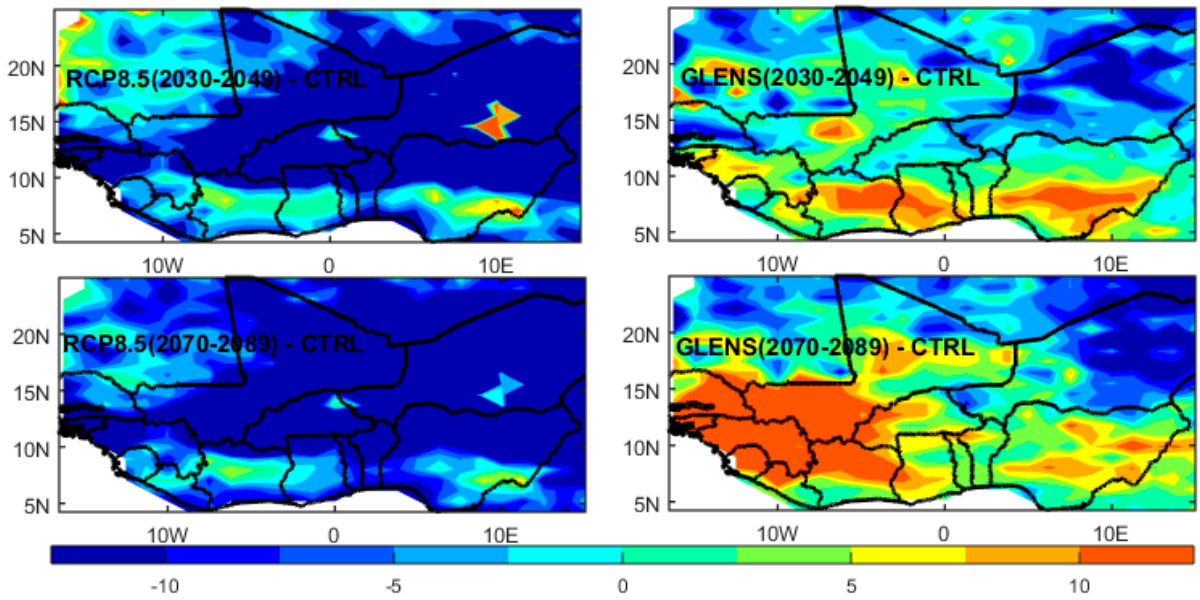

Figure 6. Change in the average of Drought duration (months) under RCP8.5 and GLENS scenarios related to Control period.

3.3.5. Maximum Length of Drought Events

Over the period 2030–2049 and under the GLENS simulations, the maximum length of drought events has been decreased in comparison to the RCP8.5 scenarios. Under the GLENS simulations, this maximum length ranges between 0 and 50 months in most regions. On the contrary, over the period 2070–2089 and under the GLENS simulations, the maximum length increases in most regions compared to the results from the RCP8.5 scenarios. This maximum length ranges between 10 and 90 months in all the countries.

Figure 7 shows the change in the maximum length of drought events under the RCP8.5 and GLENS scenarios related to the Control period. The maximum length of drought events is expected to decrease by about 0 to 80 months under RCP8.5 simulations over both the 2030–2049 and 2070–2089 projected periods related to the Control period in West Africa. This decrease could be important during the period of 2070–2089 compared to the period of 2030–2049. Under GLENS, a decrease in the maximum length of drought events is expected in Northern West Africa for both the 2030–2049 and 2070–2089 projected periods related to the Control period. For the Southern part of West Africa, an increase in the maximum length of drought events is expected. This increase could be important over 2070–2089 compared to the 2030–2049 period.

3.3.6. Severity of the Greatest Drought Event

Over the period 2030–2049 and under the GLENS simulations, the severity of the greatest drought event is less than the severity of the greatest drought events under RCP8.5 scenarios. Under the GLENS simulations, the severity of the greatest drought event ranges between 0 and 80 in most regions, whereas the severity of the greatest drought event can reach 100 is some areas of Mali and Niger under the RCP8.5 scenarios. Over the period 2070–2089 and under the GLENS simulations, the severity of the greatest drought event is higher than the severity of the greatest drought event under the RCP8.5 scenario in most regions. This severity of the greatest drought event ranges between 10 and 100 under the GLENS simulation while it varies between 0 and 40 under the RCP8.5 scenario.

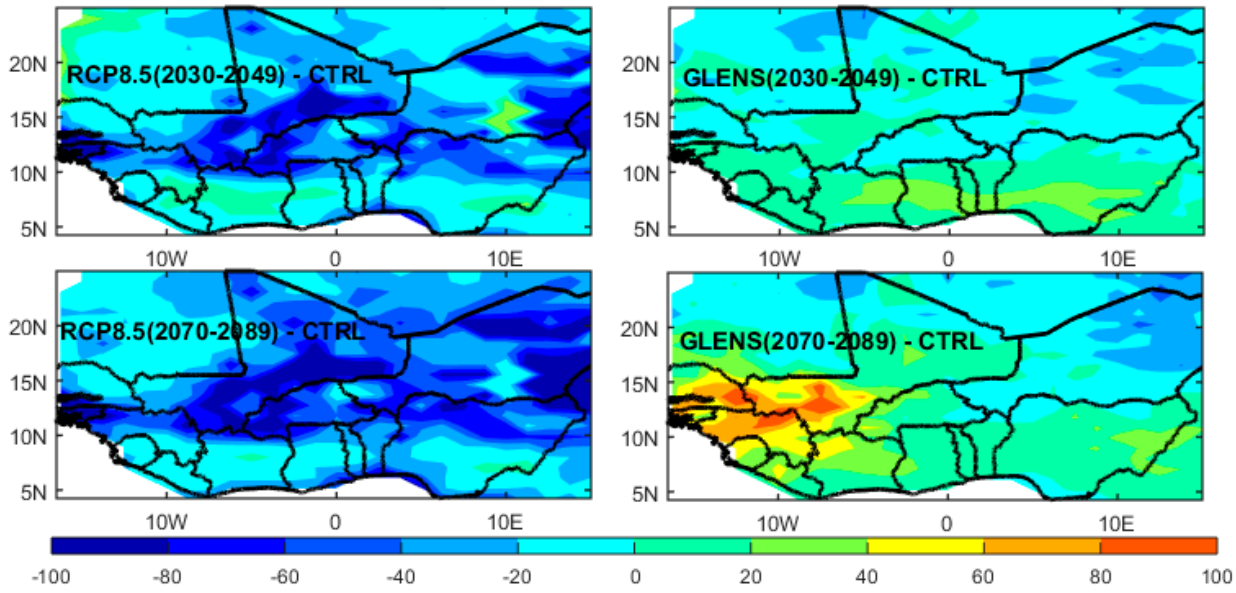

Figure 7. Change in the maximum length of drought events (months) under RCP8.5 and GLENS scenarios compared to Control period.

Figure 8 shows the severity of the greatest drought event under the RCP8.5 and GLENS scenarios. The severity of the greatest drought event is expected to decrease by about 0 to 100 under the RCP8.5 simulations over both the 2030–2049 and 2070–2089 projected periods related to the Control period in West Africa. This decrease could be important during the period of 2070–2089 compared to the period of 2030–2049. Under GLENS, a decrease in the severity of the greatest drought event is expected in Northern West Africa for both the 2030–2049 and 2070–2089 projected periods related to the Control period. For the Southern part of West Africa, an increase in the severity of the greatest drought event is expected. This increase could be important over 2070–2089 compared to the 2030–2049 period.

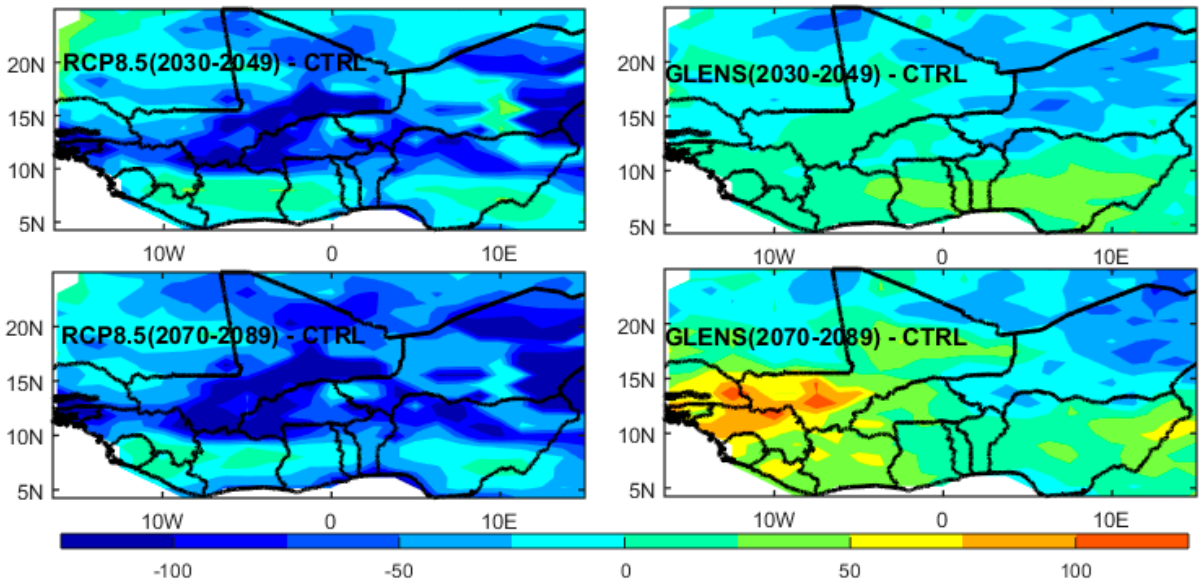

Figure 8. Change in severity of the greatest drought event under RCP8.5 and GLENS scenarios related to the Control period.

3.3.7. Intensity of the Greatest Drought Event

Over the period 2030–2049 and under the GLENS simulations, the intensities of the greatest drought events vary between one and two, indicating that the scale of the greatest drought under GLENS varies from moderate drought to extreme drought. However, the areas of extent of severe and extreme droughts are much larger than the area of moderate drought. Under RCP8.5, severe and extreme drought are expected to characterize the greatest drought in Northern West Africa, while in the southern (from Senegal to Benin) countries, there is no drought event.

Over the period 2070–2089 and under the GLENS simulations, the intensity of the greatest drought varies from 1 to 2. This indicates that the greatest drought would be moderate, severe or extreme drought. Severe and extreme drought could dominate in the large area of West Africa. Moderate drought could be found only in the north of Nigeria, in Guinea and in the east of Senegal. Under RCP8.5, the greatest drought event could be moderate in the north of West Africa, except in Mauritania, where severe and extreme moderate droughts were found. The same drought scales were also found in the large part of the south of West Africa.

Figure 9 depicts the change in the intensities of the greatest drought event under the RCP8.5 and GLENS scenarios. Changes in the intensities of the greatest drought event under RCP8.5 and GLENS scenarios related to the Control period indicate the same pattern as for the others drought characteristics. A decrease in the intensity of the greatest drought is expected under the RCP8.5 scenario while an increase in intensity is projected under the GLENS simulation in Southern West Africa.

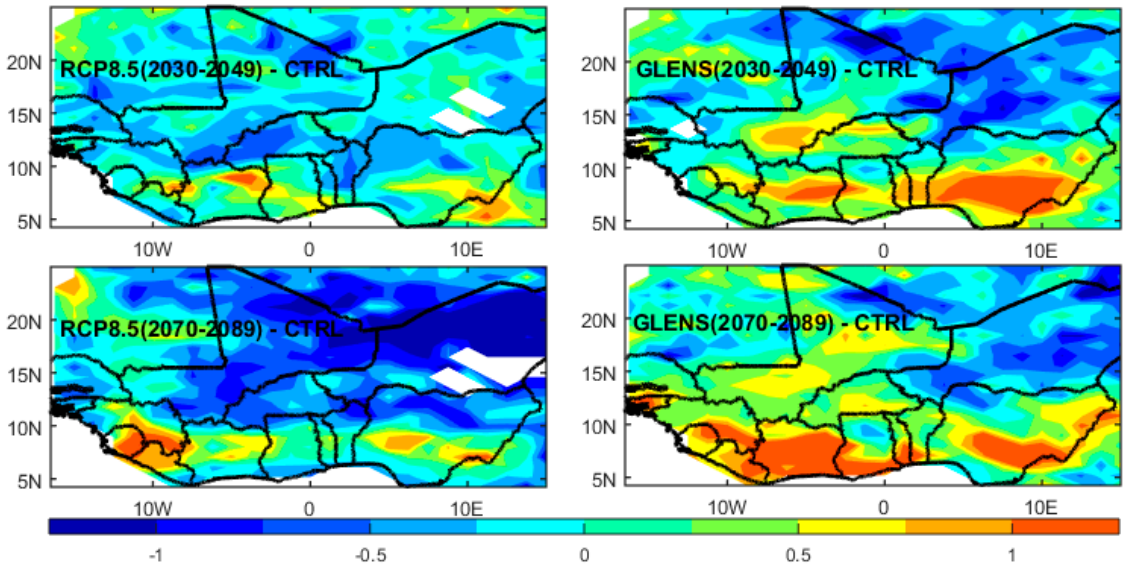

Figure 9. Change in the intensity of the greatest drought event under RCP8.5 and GLENS scenarios related to the Control period.

3.4. Cause of Change in Drought Characteristic under RCP8.5 and GLENS Scenarios

In Section 3.2, we found that projected SPI from RCP8.5 scenario have an increasing trend while projected SPI from GLENS simulation have a decreasing trend. These trends could probably be linked to annual precipitation trends under each scenario. To find the associated cause of meteorological drought change, it is important to investigate the cause of precipitation change under both RCP8.5 and GLENS scenarios. The authors of [43] decomposed precipitation changes into their thermodynamic component (driven by changes in specific humidity), dynamic component (driven by changes in the tropical circulation) and nonlinear cross component (driven by both changes in specific humidity and circulation that is negligible). Like these authors, we investigate changes in near surface specific humidity and 957 hPa wind fields to explain changes in drought characteristic in

West Africa under SAG (Figure 10). Under RCP8.5, near surface specific humidity increases related to the control (CRTL) period. This increase in near surface specific humidity contributes to intensifying climatological precipitation patterns under global warming [43]. Under GLENS, the near surface specific humidity slightly decreases related to the control period. Contrary to RCP8.5, the change in the near surface specific humidity is small under GLENS, and it could make negligible contributions to rainfall decrease. General circulation could therefore play a key role in the decrease in precipitation under GLENS. We found in Figure 10 that under GLENS there is a weakening of the winds coming from the oceanic basin (in red circle on Figure 10). As the solar radiation varies with the season and land would warm or cool faster than the ocean (due to the heat capacity of water, which is more important than that of the land), the low-level land–sea thermal contrast is strongly influenced by solar radiation [44]. The objective of the GLENS simulations is to reduce the sunlight that reaches the land and sea surface by injecting SO_2 particles into the low stratosphere. SO_2 particles have the ability to reflect a part of the incident radiation into the atmosphere. As a result, we will warm the Earth less, and therefore, we will reduce the low-level land–sea thermal contrast. The reduction of the land–sea thermal contrast leads to weak monsoon winds [43] and a slight southward shift of the ITCZ (by around 0.18°) relative to the baseline [45]. In sum, under GLENS, decreases in precipitation (increase in drought) are probably largely driven by weakened monsoon circulation due to the reduction of the land–sea thermal contrast in the lower troposphere.

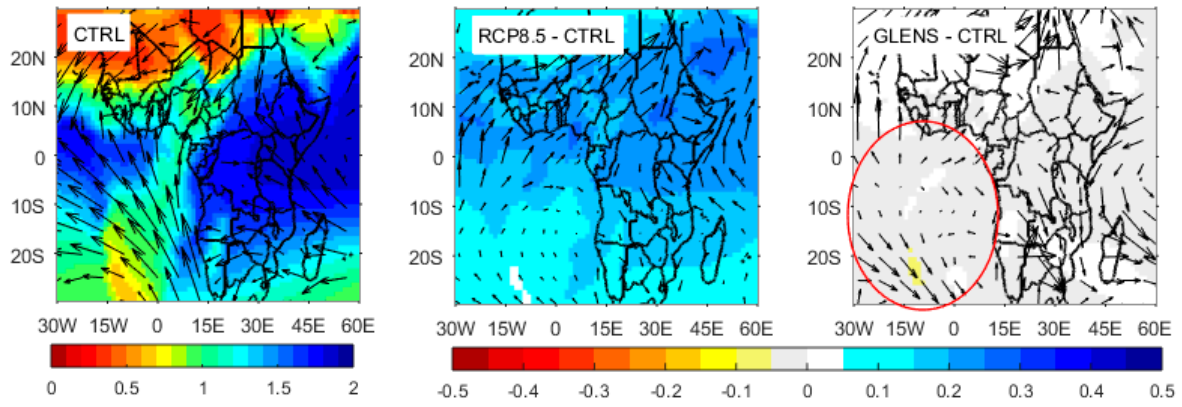

Figure 10. Spatial pattern of annual surface specific humidity (color shading) and 957 hPa wind field (vectors) for the control period and changes (relative to the control) in mean annual surface specific humidity (color shading) and 957 hPa wind field (vectors) under RCP8.5 and GLENS. The units are 10^{-2} kg. kg for specific humidity and m s^{-1} for wind speed.

4. Discussion

The projected SPI from the RCP8.5 scenario indicates an increasing trend of SPI from 2010 to 2097, while a decreasing trend is expected from the GLENS simulations. These trends mean that annual precipitation could have an increasing trend under RCP8.5 in West Africa, while under the GLENS scenario, the annual precipitation trend could become a decreasing trend. Some studies [43,45] assessed changes in precipitation under the GLENS and RCP8.5 scenarios and concluded that SAG reduces precipitation compared to RCP8.5. The decreasing trend of SPI under GLENS could intensify drought conditions in the far future in West Africa.

Moreover, it seems that the Hurst phenomenon [46] or long-term persistence (LTP) is apparent and preserved throughout RCP8.5 and GLENS. It has been shown that the LTP behavior has been detected in most key hydrological-cycle processes [4] for global scale and [47,48] at Benin (West Africa) scale. On one hand, the impact of the LTP behavior in hydroclimatic processes can highly increase the variability of the processes and thus the evaluation of the uncertainty. On the other hand, under the GLENS scenario, dry years would be more and more frequent due to long-term memory, while under the

RCP8.5 scenario, wet years would be more and more frequent. The LTP effect describes the tendency of the wet/dry years to cluster into wet/drought periods [49]. It appears important to extend the study of long-term persistence to the other hydroclimatic variables in order to establish the link between these variables' variability and drought.

Assessing the evolution of the drought area, we found that the extent area for all drought scales (DA, D_0, D_1, D_2, D_3 and D_4) have decreasing trends under the RCP8.5 simulation and increasing trends under the GLENS simulation. The projected change in drought area has shown an increase in all drought characteristics by the end of the 21st century under GLENS. In addition, the number of drought events, drought duration, drought maximum length of drought and intensity and severity of the greatest drought event were used for analyzing the future spatial drought changes. The projected change has also shown an increase in these drought characteristics by the end of the 21st century under GLENS. This suggests that West Africa will face unprecedented increases in drought characteristics under the GLENS scenario if drought mitigation and adaptation mechanisms are inadequate or missing. For this, an effective land management practice could be introduced in the region to reduce the amount of water loss due to SAG condition. This is very important because West Africa is particularly vulnerable to drought conditions. For example, the Sahelian drought of the 1970s–1990s was one of the largest humanitarian disasters of the past 50 years, causing up to 250,000 deaths and creating 10 million refugees [29].

To find the associated cause of meteorological drought change, it is important to investigate the cause of precipitation change under GLENS scenarios. Under GLENS, winds from the oceanic basin to the continent are weak compared to RCP8.5. A decrease in surface specific humidity under GLENS compared to RCP8.5 is also noted. The authors of [43] identified the physical mechanisms behind changes in West African Summer Monsoon (WASM) precipitation under RCP8.5 and GLENS by applying the decomposition method developed in [50,51]. They found that under GLENS, decreases in rainfall relative to the baseline are mainly determined by the reduction of the land–sea thermal contrast in the lower troposphere that leads to weakened monsoon circulation and a northward shift in the monsoon precipitation. However, the increase in precipitation under global warming is mostly driven by the increase in near surface specific humidity.

5. Conclusions

As most people in West Africa are involved in climate-sensitive sectors of the economy, any change in climate that encourages drier conditions may increase the vulnerability of climate risks over the region. Any substantial rainfall deficit usually devastates socio-economic activities for a long period because agriculture, hydro-electric power and river basin management depend on rainfall. Our results indicate that SAG could lead to the intensification of drought in West Africa in the future. This implies that before the deployment of SAG, the technique of injection must be improved, or new strategies are needed for stratospheric aerosol injection to attenuate rainfall changes in this region under SAG. More work has to be done in order take in account the evaporation/runoff (hydrometeorological drought) in drought assessment and to identify the impacts of drought increases under SAG on society, for example, on food production and water availability, which needs to be clarified in future studies.

Author Contributions: Conceptualization, A.E.A., E.O., E.I.B. and E.B.J.Z.; methodology, A.E.A., E.O., E.I.B., E.B.J.Z., C.Y.D.-A. and F.K.B.; software, E.O.; formal analysis, A.E.A., E.O., E.I.B. and E.B.J.Z.; writing—original draft preparation, A.E.A.; writing—review and editing, E.O.; supervision, E.B., P.J.I. and S.T.; project administration, E.B. and A.E.A. All authors have read and agreed to the published version of the manuscript.

Funding: This work has been made under the financial support of the DECIMALS fund of the Solar Radiation Management Governance Initiative (SRMGI), which was set up in 2010 by the Royal Society Environmental Defense Fund and the World Academy of Sciences (TWAS), and is funded by the Open Philanthropy Project.

Institutional Review Board Statement: Not applicable.

Informed Consent Statement: Not applicable.

Data Availability Statement: The data used in this study are available to the community via the Earth System Grid.

Acknowledgments: The authors thank the National Center for Atmospheric Research (NCAR) for the provided data. We would also like to thank the anonymous reviewers for their constructive comments and suggestions.

Conflicts of Interest: The authors declare no conflict of interest.

References

1. Haile, G.G.; Tang, Q.; Hosseini-Moghari, S.; Liu, X.; Gebremicael, T.G.; Leng, G.; Kebede, A.; Xu, X.; Yun, X. Projected Impacts of Climate Change on Drought Patterns over East Africa. *Earth's Future* **2020**. [CrossRef]
2. Touma, D.; Ashfaq, M.; Nayak, M.; Kao, S.-C.; Diffenbaugh, N. A multi-model and multi-index evaluation of drought characteristics in the 21st century. *J. Hydrol.* **2015**, *526*, 196–207. [CrossRef]
3. United Nations. *Departament of Economic and Social Affairs, Population Division, Key Findings and Advance Tables*; World Population Prospects: London, UK, 2017.
4. Dimitriadis, P.; Koutsoyiannis, D.; Iliopoulou, T.; Papanicolaou, P. A global-scalen investigation of stochastic similarities in marginal distribution and dependence structure of key hydrological-cycle processes. *Hydrology* **2021**, *8*, 59. [CrossRef]
5. Koutsoyiannis, D. Revisiting the global hydrological cycle: Is it intensifying? *Hydrol. Earth Syst. Sci.* **2020**, *24*, 3899–3932. [CrossRef]
6. Wang, J.-W.; Wang, K.; Pielke, R.; Lin, J.C.; Matsui, T. Towards a robust test on North America warming trend and precipitable water content increase. *Geophys. Res. Lett.* **2008**, *35*, 18804. [CrossRef]
7. Chattopadhyay, S.; Edwards, D.R.; Yu, Y.; Hamidisepehr, A. An Assessment of climate change impacts on future water availability and droughts in the Kentucky river basin. *Environ. Process.* **2017**, *4*, 477–507. [CrossRef]
8. IPCC. *Impacts, Adaptation, and Vulnerability, Part A: Global and Sectoral Aspects: Working Group II to the Fifth Assessment Report of the Intergovernmental Panel on Climate Change*; Field, C.B., Barros, V.R., Dokken, D.J., Mach, K.J., Mastrandrea, M.D., Bilir, T.E., Chatterjee, M., Ebi, K.L., Estrada, Y.O., Genova, R.C., et al., Eds.; Cambridge University Press: Cambridge, UK; New York, NY, USA, 2014; p. 1132.
9. Robock, A. Reply to comment on "the latest on the volcanic eruptions and climate". *EOS* **2014**, *95*, 353. [CrossRef]
10. Crutzen, P.J. Albedo enhancement by stratospheric sulfur injections: A contribution to resolve a policy dilemma? *Clim. Chang.* **2006**, *77*, 211–220. [CrossRef]
11. Irvine, P.; Emanuel, K.; He, J.; Horowitz, L.W.; Vecchi, G.; Keith, D. Halving warming with idealized solar geoengineering moderates key climate hazards. *Nat. Clim. Chang.* **2019**, *9*, 295–299. [CrossRef]
12. Jiang, J.; Cao, L.; MacMartin, D.; Simpson, I.R.; Kravitz, B.; Cheng, W.; Visioni, D.; Tilmes, S.; Richter, J.H.; Mills, M.J. Stratospheric sulfate aerosol geoengineering could alter the high-latitude seasonal cycle. *Geophys. Res. Lett.* **2019**, *46*, 14153–14163. [CrossRef]
13. Jones, A.C.; Hawcroft, M.K.; Haywood, J.M.; Jones, A.; Guo, X.; Moore, J.C. Regional climate impacts of stabilizing global warming at 1.5 k using solar geoengineering. *Earth's Future* **2018**, *6*, 230–251. [CrossRef]
14. Kravitz, B.; Caldeira, K.; Boucher, O.; Robock, A.; Rasch, P.J.; Alterskjaer, K.; Karam, D.B.; Cole, J.; Curry, C.; Haywood, J.M.; et al. Climate model response from the Geoengineering Model Intercomparison Project (GeoMIP). *J. Geophys. Res. Atmos.* **2013**, *118*, 8320–8332. [CrossRef]
15. MacMartin, D.G.; Wang, W.; Kravitz, B.; Tilmes, S.; Richter, J.H.; Mills, M.J. Timescale for detecting the climate response to stratospheric aerosol geoengineering. *J. Geophys. Res. Atmos.* **2019**, *124*, 1233–1247. [CrossRef]
16. Tilmes, S.; Richter, J.H.; Kravitz, B.; MacMartin, D.G.; Mills, M.J.; Simpson, I.R.; Glanville, A.; Fasullo, J.T.; Phillips, A.S.; Lamarque, J.-F.; et al. CESM1(WACCM) stratospheric aerosol geoengineering large ensemble project. *Bull. Am. Meteorol. Soc.* **2018**, *99*, 2361–2371. [CrossRef]
17. Pinto, I.; Jack, C.; Lennard, C.; Tilmes, S.; Odoulami, R. Africa's Climate Response to Solar Radiation Management with Stratospheric Aerosol. *Am. Geophys. Res. Lett.* **2020**, *47*. [CrossRef]
18. Bala, G.; Duffy, P.B.; Taylor, K.E. Impact of geoengineering schemes on the global hydrological cycle. *Proc. Natl. Acad. Sci. USA* **2008**, *105*, 7664–7669. [CrossRef] [PubMed]
19. Robock, A.; Oman, L.; Stenchikov, G.L. Regional climate responses to geoengineering with tropical and arctic SO_2 injections. *J. Geophys. Res. Earth Surf.* **2008**, *113*, 16101. [CrossRef]
20. Tilmes, S.; Fasullo, J.; Lamarque, J.-F.; Marsh, D.R.; Mills, M.; Alterskjaer, K.; Muri, H.; Kristjánsson, J.E.; Boucher, O.; Schulz, M.; et al. The hydrological impact of geoengineering in the Geoengineering Model Intercomparison Project (GeoMIP). *J. Geophys. Res. Atmos.* **2013**, *118*, 11036–11058. [CrossRef]
21. Kravitz, B.; MacMartin, D.G.; Mills, M.J.; Richter, J.H.; Tilmes, S.; Lamarque, J.; Tribbia, J.J.; Vitt, F. First simulations of designing stratospheric sulfate aerosol geoengineering to meet multiple simultaneous climate objectives. *J. Geophys. Res. Atmos.* **2017**, *122*, 12616–12634. [CrossRef]

22. Niemeier, U.; Schmidt, H.; Alterskjaer, K.; Kristjánsson, J.E. Solar irradiance reduction via climate engineering: Impact of different techniques on the energy balance and the hydrological cycle. *J. Geophys. Res. Atmos.* **2013**, *118*, 11905–11917. [CrossRef]
23. Quenum, G.M.L.D.; Klutse, N.A.B.; Dieng, D.; Laux, P.; Arnault, J.; Kodja, J.D.; Oguntunde, P.G. Identification of potential drought areas in West Africa under climate change and variability. *Earth Syst. Environ.* **2019**, *3*, 429–444. [CrossRef]
24. Oguntunde, P.G.; Abiodun, B.J.; Lischeid, G.; Abatan, A.A. Droughts projection over the Niger and Volta River basins of West Africa at specific global warming levels. *Int. J. Clim.* **2020**, *40*, 1–12. [CrossRef]
25. Kasei, R.; Diekkrüger, B.; Leemhuis, C. Drought frequency in the Volta Basin of West Africa. *Sustain. Sci.* **2010**, *5*, 89–97. [CrossRef]
26. Oguntunde, P.G.; Lischeid, G.; Abiodun, B.J. Impacts of climate variability and change on drought characteristics in the Niger River Basin, West Africa. *Stoch. Environ. Res. Risk Assess.* **2018**, *32*, 1017–1034. [CrossRef]
27. Oguntunde, P.; Abiodun, B.J.; Lischeid, G. Impacts of climate change on hydro-meteorological drought over the Volta Basin, West Africa. *Glob. Planet. Chang.* **2017**, *155*, 121–132. [CrossRef]
28. Adaawen, S. Understanding Climate change and drought perceptions, impact and responses in the rural savannah, West Africa. *Atmosphere* **2021**, *12*, 594. [CrossRef]
29. Haywood, J.M.; Jones, A.; Bellouin, N.; Stephenson, D.B. Asymmetric forcing from stratospheric aerosols impacts Sahelian rainfall. *Nat. Clim. Chang.* **2013**, *3*, 660–665. [CrossRef]
30. Onojeghuo, A.R.; Heiko, B.; Monks, P.S. Tropospheric NO_2 concentrations over West Africa are influenced by climate zone and soil moisture variability. *Atmos. Chem. Phys. Discuss.* **2017**. [CrossRef]
31. Ly, M.; Traore, B.S.; Alhassane, A.; Sarr, B. Evolution of some observed climate extremes in the West African Sahel. *Weather. Clim. Extrem.* **2013**, *1*, 19–25.
32. Mills, M.J.; Schmidt, A.; Easter, R.; Solomon, S.; Kinnison, D.E.; Ghan, S.J.; Marhs, D.R.; Lamarque, J.-F.; Calvo, N.; Polvani, L.M. Global volcanic aerosol properties derived from emissions, 1990–2014, using CESM1(WACCM). *J. Geophys. Res. Atmos.* **2016**, *121*, 2332–2348. [CrossRef]
33. Farahmand, A.; AghaKouchak, A. A generalized framework for deriving nonparametric standardized drought indicators. *Adv. Water Resour.* **2015**, *76*, 140–145. [CrossRef]
34. Koutsoyiannis, D. *Stochastics of Hydroclimatic Extremes. A Cool Look at Risk*; Kallipos: Athens, Greece, 2021; 333p, ISBN 978-618-85370-0-2.
35. Kumar, M.N.; Murthy, C.S.; Sai, M.V.R.S.; Roy, P.S. On the use of standardized precipitation index (SPI) for drought intensity assessment. *Meteorol. Appl.* **2009**, *16*, 381–389. [CrossRef]
36. Quiring, S.M. Developing Objective Operational Definitions for Monitoring Drought. *J. Appl. Meteorol. Clim.* **2009**, *48*, 1217–1229. [CrossRef]
37. Turnbull, B.W. The Empirical Distribution Function with Arbitrarily Grouped, Censored and Truncated Data. *J. R. Stat. Soc. Ser. B* **1976**, *38*, 290–295. [CrossRef]
38. Gringorten, I.I. A plotting rule for extreme probability paper. *J. Geophys. Res. Earth Surf.* **1963**, *68*, 813–814. [CrossRef]
39. Hao, Z.; AghaKouchak, A.; Nakhjiri, N.; Farahmand, A. Global integrated drought monitoring and prediction system. *Sci. Data* **2014**, *1*, 140001. [CrossRef] [PubMed]
40. Akinsanola, A.A.; Ogunjobi, K.O.; Gbode, I.E.; Ajayi, V.O. Assessing the capabilities of three regional climate models over CORDEX Africa in simulating West African summer monsoon precipitation. *Adv. Meteorol.* **2015**, *2015*, 935431. [CrossRef]
41. Akinsanola, A.A.; Zhou, W. Ensemble-based CMIP5 simulations of West African summer monsoon rainfall: Current climate and future changes. *Theor. Appl. Clim.* **2019**, *136*, 1021–1031. [CrossRef]
42. Diallo, I.; Giorgi, F.; Tall, M.; Mariotti, L.; Gaye, A.T. Projected changes of summer monsoon extreme and hydro-climatic regimes over West Africa for the twenty-first century. *Clim. Dyn.* **2016**, *47*, 3931–3954. [CrossRef]
43. Da-Allada, C.Y.; Baloïtcha, E.; Alamou, E.A.; Awo, F.M.; Bonou, F.; Pomalegni, Y.; Biao, E.I.; Obada, E.; Zandagba, J.E.; Tilmes, S.; et al. Changes in West African summer monsoon precipitation under stratospheric aerosol geoengineering. *Earth's Future* **2020**, *8*, e2020EF001595. [CrossRef]
44. Liu, Y.; Cai, W.; Sun, C.; Song, H.; Cobb, K.M.; Li, J.; Leavitt, S.W.; Wu, L.; Cai, Q.; Liu, R.; et al. Anthropogenic aerosols cause recent pronounced weakening of asian summer monsoon relative to last four centuries. *Geophys. Res. Lett.* **2019**, *46*, 5469–5479. [CrossRef]
45. Hurst, H.E. Long-term storage capacity of reservoirs. *Trans. Am. Soc. Civ. Eng.* **1951**, *116*, 770–799. [CrossRef]
46. Biao, E.I.; Alamou, E.A. Influence of the long-range dependence in rainfall in modelling oueme river basin (Benin, West Africa). *Am. J. Biol. Environ. Stat.* **2016**, *2*, 50–59. [CrossRef]
47. Obada, E.; Alamou, E.A.; Biao, E.I.; Afouda, A. On the use of simple scaling stochastic (SSS) framework to the daily hydroclimatic time series in the context of climate change. *Hydrology* **2016**, *4*, 35. [CrossRef]
48. Sakalauskiene, G. The hurst phenomenon in hydrology. *Environ. Res. Eng. Manag.* **2003**, *3*, 16–20.
49. Cheng, W.; MacMartin, D.G.; Dagon, K.; Kravitz, B.; Tilmes, S.; Richter, J.H.; Mills, M.J.; Simpson, I.R. Soil moisture and other hydrological changes in a stratospheric aerosol geoengineering large ensemble. *J. Geophys. Res. Atmos.* **2019**, *124*, 12773–12793. [CrossRef]
50. Chadwick, R.; Good, P.; Willett, K. A simple moisture advection model of specific humidity change over land in response to SST warming. *J. Clim.* **2016**, *29*, 7613–7632. [CrossRef]
51. Chadwick, R.; Boutle, I.; Martin, G. Spatial Patterns of Precipitation Change in CMIP5: Why the Rich Do Not Get Richer in the Tropics. *J. Clim.* **2013**, *26*, 3803–3822. [CrossRef]